Overscreening and Underscreening in Solid-Electrolyte Grain Boundary Space-Charge Layers

Jacob M. Dean,[1,2] Samuel W. Coles,[1,2,*] William R. Saunders,[3] Andrew R. McCluskey,[4,1] Matthew J. Wolf,[3] Alison B. Walker,[3] and Benjamin J. Morgan[1,2,†]

[1]Department of Chemistry, University of Bath, Claverton Down BA2 7AY, United Kingdom
[2]The Faraday Institution, Quad One, Harwell Science and Innovation Campus, Didcot OX11 0RA, United Kingdom
[3]Department of Physics, University of Bath, Claverton Down BA2 7AY, United Kingdom
[4]European Spallation Source ERIC, P.O. Box 176, SE-221 00, Lund, Sweden

(Received 2 April 2021; accepted 17 August 2021; published 24 September 2021)

Polycrystalline solids can exhibit material properties that differ significantly from those of equivalent single-crystal samples, in part, because of a spontaneous redistribution of mobile point defects into so-called space-charge regions adjacent to grain boundaries. The general analytical form of these space-charge regions is known only in the dilute limit, where defect-defect correlations can be neglected. Using kinetic Monte Carlo simulations of a three-dimensional Coulomb lattice gas, we show that grain boundary space-charge regions in nondilute solid electrolytes exhibit overscreening—damped oscillatory space-charge profiles—and underscreening—decay lengths that are longer than the corresponding Debye length and that increase with increasing defect-defect interaction strength. Overscreening and underscreening are known phenomena in concentrated liquid electrolytes, and the observation of functionally analogous behavior in solid electrolyte space-charge regions suggests that the same underlying physics drives behavior in both classes of systems. We therefore expect theoretical approaches developed to study nondilute liquid electrolytes to be equally applicable to future studies of solid electrolytes.

DOI: 10.1103/PhysRevLett.127.135502

Predicting the equilibrium distribution of charged ions within crystalline solids at, or near, structural discontinuities such as grain boundaries or heterointerfaces is a long-standing problem in solid-state physics [1–6]. Within these near-interface regions, the concentration of individual ionic species can deviate significantly from their formal bulk values, giving rise to so-called "space-charge" regions. The spatial profiles of space-charge regions are particularly significant in solid electrolytes [7,8] such as those used in solid-oxide fuel cells and all–solid-state lithium ion batteries [5,6,9,10]. In these cases, a local decrease in the concentration of the charge-carrying mobile ionic species within a space-charge region is expected to contribute to interfacial resistance and decreased device performance [7,11,12].

The classic treatment of space-charge formation in solid electrolytes considers the distribution of mobile ions in terms of charge-carrying point defects—typically interstitials or vacancies—that behave as an ideal gas interacting only through mean-field electrostatics [7]. For this simple model, the equilibrium defect distribution perpendicular to the grain boundary interface can be found by solving the one-dimensional Poisson-Boltzmann equation. For low space-charge potentials [13], the approximate linearized Poisson-Boltzmann equation can be used, which has a general analytical solution; the resulting space-charge profiles decay exponentially toward the asymptotic bulk defect concentration with a characteristic decay length equal to the Debye length λ_D:

$$\lambda_D = \sqrt{\frac{\varepsilon_0 \varepsilon_r k_B T}{\sum_i (z_i e)^2 c_i}}, \tag{1}$$

where ε_0 is the vacuum permittivity, ε_r is the relative permittivity of the solid, k_B is the Boltzmann constant, T is the temperature, z_i are the charged species' valences, e is the elementary charge, and c_i are the bulk charged defect concentrations. For high space-charge potentials, the full nonlinear Poisson-Boltzmann equation must be solved, either numerically or by making further approximations to obtain an approximate analytical result [14]. Space-charge profiles for high space-charge potentials again decay monotonically, exhibiting superexponential decay close to the grain boundary, converging to exponential decay with decay length λ_D at larger distances.

This ideal-gas plus mean-field–electrostatics model of space-charge behavior is valid only in the dilute limit of low defect density or high relative permittivity, i.e., weak electrostatic coupling. To address this limitation, a number of more complex one-dimensional models have been proposed that aim to describe space-charge behavior under nondilute conditions [10,14–18]. These models extend the simple model described above by including additional nonideal local or nonlocal defect chemical potential terms. The equilibrium space-charge profile is then computed by minimizing the global free energy as a function of the one-dimensional defect concentration. These extended models can give complex nonexponential or even nonmonotonic space-charge profiles, although the exact functional form of the resulting profile depends on the choice of nonideal chemical potential terms and their parameterization.

As is the case for the classic space-charge model, these nondilute space-charge models solve a one-dimensional problem defined in terms of the mobile-defect density perpendicular to the interfacial plane. Each point in this one-dimensional density can be considered a planar average from some corresponding implicit three-dimensional defect distribution; the full three-dimensional distribution of mobile defects within the solid-electrolyte host, however, is never explicitly calculated. As a consequence, defect-defect correlations, which become increasingly important with increasing defect concentration or decreasing relative permittivity, are not explicitly computed. Instead, the effect of these correlations is approximated through the choice of nonideal defect chemical potential terms used in each model.

Here, we follow a different approach to modeling solid-electrolyte space-charge profiles. Instead of solving an effective one-dimensional problem, we consider an explicit three-dimensional Hamiltonian for point charges in a system with a single grain boundary. We then sample the configuration space of this model, using kinetic Monte Carlo, and construct space-charge profiles as time averages over specific simulation trajectories. Because this approach treats defect-defect interactions explicitly in three-dimensional space, any defect-defect correlations emerge directly from the simulation trajectories, avoiding the need to describe these correlations through analytical free-energy terms.

We find that in nondilute solid electrolytes (high defect concentrations) or for strong defect-defect interactions (low relative permittivities) grain-boundary–adjacent space-charge profiles have a qualitatively different functional form to the monotonic decay predicted by classic space-charge theory. We observe damped oscillatory space-charge profiles that can be well described by a simple analytical function. We also observe space-charge decay lengths that are significantly larger than the corresponding Debye length and that increase with increasing defect concentration or defect-defect interaction strength (decreasing relative permittivity), giving the opposite behavior to that predicted by dilute-limit models. The deviation of space-charge decay length from the Debye length is shown to follow a universal scaling law as a function of electrostatic coupling strength. We note that analogous phenomena have been previously reported for concentrated liquid electrolytes, which suggests that the same underlying physics drives emergent behavior in solid electrolytes as in their liquid counterparts. Finally, we comment on the implications of these results for a possible unified theoretical framework for understanding nondilute electrolyte behavior in both liquids and solids.

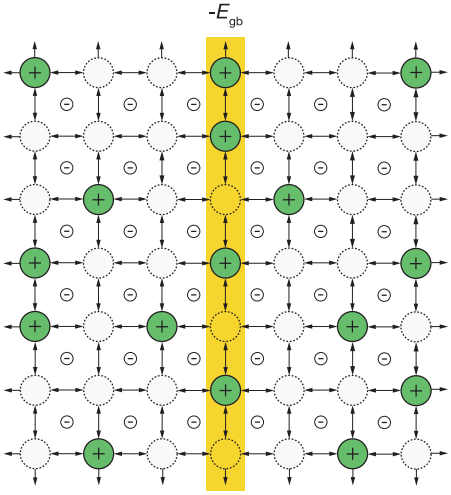

FIG. 1. Two-dimensional schematic of the kinetic Monte Carlo model used in this work. Lattice sites (circles) are either vacant (dashed circles) or occupied by positively charged "defects" (solid green circles). Arrows indicate allowed site-site moves. Interstitial positions are assigned partial negative charges. All lattice sites in the central plane (yellow) are assigned an on-site occupation energy of $-E_{gb}$.

Methods.—Our computational model consists of a 3D-periodic simple-cubic lattice of $m \times m \times m$ sites, populated by a fixed number, N, of mobile point defects with $+1$ charge (Fig. 1). To ensure our model has net zero charge, we include a uniform array of δ^- point charges located at the cube-center–interstitial positions, with $\delta^- = -N/m^3$. The mobile defects and their countercharges interact through point-charge electrostatics, which we scale by a relative permittivity ε_r. This Coulomb lattice-gas model has historically been well studied as a bulk system [19], particularly in the context of the classical one-component plasma [20,21]. To model the segregation of mobile defects to a grain boundary, we assign one plane of sites an on-site occupation energy of $-E_{gb}$; this term represents the difference in standard chemical potential or "segregation energy" for defects in the grain boundary core relative to the bulk. All sites outside the grain boundary core have on-site energies of zero.

Our kinetic Monte Carlo simulations were performed using the KMC_FMM code, which implements the accurate

and optimally scaling electrostatic solver described in Ref. [22] using the PPMD framework [23]. All simulations were performed using a $75 \times 75 \times 75$ simple-cubic lattice of sites, with three-dimensional periodic boundary conditions. The nearest-neighbour mobile-site spacing, l, is 2.5 Å, which approximates the typical lattice spacing of a solid electrolyte. For all simulations, we set the on-site occupation energy for the grain boundary plane as $-E_{\mathrm{gb}} = -0.05$ eV. Simulations were run at 300 K. Each individual simulation was initialized with a random distribution of mobile charges and run for a total of 1.5×10^6 steps. The initial 500 000 steps were discarded to allow for equilibration, and space-charge profiles were computed as a time average over the subsequent 1×10^6 steps. For each combination of relative permittivity, ε_r, and bulk concentration, c_∞, we performed between 30 and 100 simulations to obtain statistically converged space-charge profiles. To characterize and quantify the simulated space-charge profiles, we performed maximum likelihood sampling, parameter posterior sampling, and Bayesian model selection for competing functional forms using the URAVU Python package [24]. The posterior distributions and Bayesian evidence for specific functional models were found by nested sampling [25], implemented in URAVU using the DYNESTY package [26]. Further details are given in the Supplemental Material [27].

Results.—We first consider simulated space-charge profiles obtained for $n_\infty = 0.005$, where $n_\infty = l^3 c_\infty$ is the bulk per-site number density of mobile defects, and $\varepsilon_r = 100$, 10, and 1 (Fig. 2), which spans the range of relative permittivities for typical solid electrolytes [10]. At higher values of ε_r, the electrostatic interaction between the mobile defects is more effectively screened, and each model will more closely approximate the noninteracting (dilute) ideal lattice-gas limit. Conversely, as ε_r is decreased, the electrostatic interactions between mobile defects become stronger and nonideal defect-defect correlations are expected to become more significant.

For the highest permittivity considered here ($\varepsilon_r = 100$), we obtain a monotonically decaying space-charge profile [Fig. 2(a)] that is qualitatively consistent with the dilute-limit behavior predicted by the classic Poisson-Boltzmann model. More precisely, the simulated space-charge profile is well described by an exponentially decaying function,

$$n(x) = n_\infty + A \exp(-\alpha x), \tag{2}$$

where $n(x)$ is the planar-average defect number density, n_∞ is the bulk defect number density, and $\alpha = 1/\lambda_{\mathrm{sys}}$, with λ_{sys} the observed characteristic decay length. At lower permittivities, the simulated space-charge profiles are no longer monotonic [Fig. 2(b)] and are therefore not even qualitatively well-described by Eq. (2). We instead observe oscillatory behavior that decays into the bulk. Further decreases in ε_r cause both the magnitude of these oscillations and the distance over which they decay to increase [Fig. 2(c)].

The appearance of oscillations at higher defect-defect interaction strengths (decreasing ε_r) mirrors the behavior of nondilute liquid electrolytes and ionic liquids, which exhibit similar oscillatory charge profiles at electrified interfaces, where this phenomenon is termed "overscreening" [30]. Oscillatory local order has also been observed in previous bulk Coulomb lattice-gas and one-component plasma simulations [20,21,31]. By analogy to the analytically known behavior of liquid systems [32,33], we propose a damped oscillatory ansatz for the space-charge profiles in this low-permittivity regime:

$$n(x) = n_\infty + A \exp(-\alpha x) \cos(\xi x + \theta). \tag{3}$$

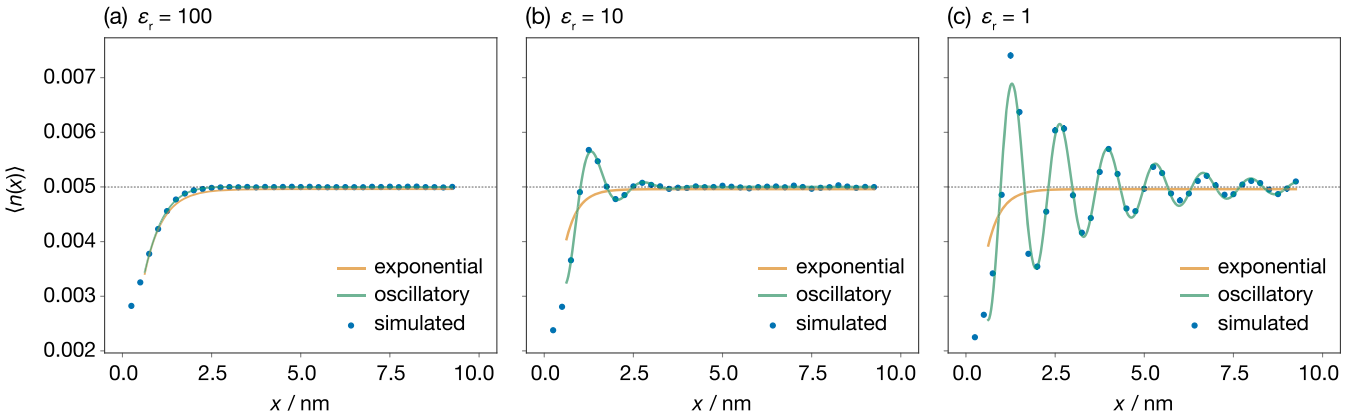

FIG. 2. One-dimensional time-averaged mobile-defect distributions for $n_\infty = 0.005$ and relative permittivities (a) $\varepsilon_r = 100$, (b) $\varepsilon_r = 10$, and (c) $\varepsilon_r = 1$. On each plot, $x = 0$ corresponds to the grain boundary plane. For each set of simulation data, we also plot the maximum likelihood exponential and oscillatory models (Eqs. (2) and (3), respectively). Error bars show a 95% confidence interval around each point (errors are smaller than the symbols). Plots showing these data on a semilogarithmic scale are provided in the Supplemental Material [27]. Source: Raw simulation data and scripts to generate this figure are available under CC BY 4.0/MIT licenses as Ref. [29].

As shown in Figs. 2(b) and 2(c), this oscillatory functional form gives a significantly better description of these space-charge profiles at low permittivities than the dilute-limit monotonic (purely exponential) model [34].

The simulated space-charge profiles presented in Fig. 2 also show *increasing* space-charge widths—i.e., increased decay lengths—with *decreasing* relative permittivities. This is the opposite behavior to that predicted by the classic space-charge treatment, wherein the Debye length decreases with decreasing ε_r [Eq. (1)]. The observation of a decay length that is larger than the classical Debye length again mirrors the behavior of concentrated liquid electrolytes, where this phenomenon is termed "underscreening" [32,33,36].

In ionic liquids and concentrated liquid electrolytes, underscreening has been found to follow scaling laws of the form

$$\left(\frac{\lambda_{\mathrm{sys}}}{\lambda_D}\right) \propto \left(\frac{d}{\lambda_D}\right)^{\nu}, \tag{4}$$

where λ_{sys} is the observed decay length of the system, d is the diameter of the charged species, and ν is a fixed scaling factor [37–40]. For our Coulomb lattice-gas model, there is no direct analog for d. We instead analyze our simulation data by plotting $\ln(\lambda_{\mathrm{sys}}/\lambda_D)$ versus $\ln(\Gamma)$, where Γ is a dimensionless parameter that describes the strength of electrostatic coupling in a given system. $\Gamma = \lambda_B/a$, where $\lambda_B = e^2/(4\pi\varepsilon_0\varepsilon_r k_B T)$ is the Bjerrum length, and $a = [3/(4\pi c_\infty)]^{1/3}$ is a Wigner-Seitz defect-sphere radius [20,21,41]. Further discussion of the choice of an appropriate scaling parameter is provided in the Supplemental Material [27].

Figure 3 shows $\ln(\lambda_{\mathrm{sys}}/\lambda_D)$ versus $\ln(\Gamma)$ plotted for simulations at four bulk concentrations corresponding to $n_\infty = 0.000\,25$, $0.000\,5$, 0.001, and 0.005. For each simulation, we use Bayesian model selection to select which model—purely exponential or damped oscillatory—is best supported by the simulated space-charge–profile data and assign $\lambda_{\mathrm{sys}} = 1/\alpha$. For $\ln(\Gamma) > 0.4$, we find analogous scaling behavior to that reported for liquid systems [32,39,40,42], i.e., $\lambda_{\mathrm{sys}}/\lambda_D \propto \Gamma^{\nu}$, with $\nu = 1.087 \pm 0.005$ (95% CI). For a given bulk concentration of mobile defects, higher values of Γ correspond to stronger defect-defect interactions, i.e., decreased ε_r. In this regime, as defect-defect interactions increase in magnitude, the observed decay length increasingly positively deviates from the Debye length. For $\ln(\Gamma) < 0.4$, we observe a region where the observed screening length is *smaller* than the Debye length. Again, this behavior has been reported for liquid systems in studies that focus on the application of different closure relationships to the Ornstein-Zernike equation [37,39,42–49]. At the lowest values of Γ (≈ 0.25, obtained for $n_\infty = 0.000\,25$ and $\varepsilon_r = 100$) we recover the low-potential dilute-limit result that the simulated decay length

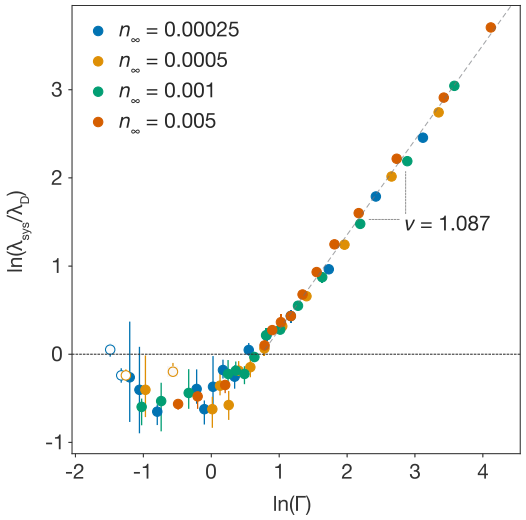

FIG. 3. Log-log plot of scaled simulated decay length $\lambda_{\mathrm{sys}}/\lambda_D = 1/(\alpha\lambda_D)$ versus $\Gamma = \lambda_B/a$ for simulations performed at four different defect concentrations. The diagonal dashed line shows the maximum likelihood estimate for Eq. (4) in the underscreening regime. Open and closed circles correspond to space-charge profiles that best support the pure exponential decay model [Eq. (2)] or the oscillatory decay model [Eq. (3)], respectively, as determined through Bayesian model selection (see the Supplemental Material [27] for details). Error bars show 95% confidence intervals for $\lambda_{\mathrm{sys}}/\lambda_D$. Source: Raw simulation data and scripts to generate this figure are available under CC BY 4.0/MIT licenses as Ref. [29].

is equal to the Debye length, i.e., $\lambda_{\mathrm{sys}} = \lambda_D$. We note that the same scaling behavior is observed for all four simulated concentrations, suggesting a universal scaling law operates in solid electrolytes that contain a single mobile-defect species.

Summary and Discussion.—We have performed kinetic Monte Carlo simulations of populations of mobile point defects on a three-dimensional lattice, interacting via point-charge electrostatics, as a simple model for space-charge formation at solid-electrolyte grain boundaries, for a range of bulk defect concentrations and relative permittivities. For dilute, weakly coupled systems (low particle concentration and high ε_r), we recover the behavior predicted by classic treatments of space-charge behavior, i.e., the linearized Poisson-Boltzmann model—the space-charge profile decays exponentially to the asymptotic bulk value with a decay length equal to the Debye length λ_D. In nondilute, strongly coupled systems (high particle concentration or low ε_r), we observe damped oscillatory space-charge profiles—overscreening—and space-charge decay lengths that are larger than the corresponding Debye length—underscreening.

Overscreening and underscreening are known phenomena for nondilute liquid systems of charged particles (concentrated liquid electrolytes and ionic liquids) [30,32,33,38,50–57]. Our simulations predict not only that

overscreening and underscreening also occur in nondilute solid electrolytes, but that these phenomena have the same functional behavior in solids as in analogous liquid systems. Space-charge profiles in systems that exhibit overscreening are well-described by a damped oscillatory function and the degree of underscreening, given by the ratio of the observed space-charge decay length to the classic Debye length, follows an apparently universal scaling law above some critical effective defect-defect interaction strength. We also predict an intermediate regime, where the simulated space-charge decay length is *smaller* than the classic Debye length. Again, this mirrors previous results obtained for the decay of radial distribution functions in nondilute liquid systems [37,39,42,49]. Our results also suggest an approximate empirical threshold for when the dilute-limit classic space-charge treatment may be reliably used to quantitatively model space-charge behavior in solid electrolytes of $\Gamma = \lambda_B/a \lessapprox 0.25$.

The strong correspondence between our results for space-charge formation at a grain boundary in a model solid electrolyte and those previously reported for liquid electrolytes at an electrified interface suggests that the same underlying physics is responsible for these analogous emergent phenomena in both liquid and solid electrolytes. This suggests that many of the theoretical methods that have been developed previously by researchers seeking to better understand the behavior of liquid electrolytes, or analogous models such as the one-component plasma [20,21], may be equally applicable to developing an improved understanding of the emergent behavior of ensembles of mobile charged defects in solid electrolytes.

Our results also present some intriguing differences with respect to previous studies of nondilute liquid systems. Our model contains a single mobile-defect species, while studies of liquid systems generally consider symmetric 1:1 electrolytes. Previous studies of liquid systems have attempted to explain ion-ion correlations and related phenomena such as overscreening in terms of ion pairing or clustering of oppositely charged ions [32,58,59]. The model presented here, however, is not charge-symmetric, and our results therefore show that charge symmetry or ion pairing are not necessary conditions for overscreening and underscreening to occur. We also observe a different scaling law for the ratio $\lambda_{\mathrm{sys}}/\lambda_D$ to that reported for liquids. In liquid systems, this scaling depends on the mean ion diameter [37–40]. In our solid-electrolyte model, there is no analogous "defect diameter" term; the Wigner-Seitz radius is independent of the identity of the mobile-defect species being considered [20,21,41]. We therefore hope that the results presented here will encourage new discussion about the origin of these empirical scaling laws in liquids in addition to our primary observation that these phenomena are also relevant in solid-state systems.

The simple grain boundary model that we have used in this work makes similar simplifying approximations to those often used in conventional one-dimensional Poisson-Boltzmann or global–free-energy treatments of grain boundary space-charge formation: all positions within the bulk crystal are energetically equivalent and the grain boundary is modeled by a uniform plane of sites [14,60–62]. Real solid electrolytes, of course, are chemically and structurally more complex. For example, immobile point defects in the bulk can affect the potential energies of mobile ions nearby [63,64], while grain boundaries can have a range of nonzero segregation energies that extend over several atomic layers [11,65,66]. Interactions between mobile defects may also be more complex than the simple point-charge interaction considered here; in some materials higher-order electrostatic terms or lattice-strain–mediated interactions may be significant at short defect-defect separations [67,68]. Accurate quantitative predictions of space-charge profiles, therefore, require the development of more detailed treatments, with one prospective route being extended Hamiltonian-based models that can be directly parameterized from first-principles calculations. While understanding the effect of these, and other, factors in real materials provides considerable scope for future investigation, we expect point-charge-like electrostatics to capture much of the physics of real systems, and therefore expect the qualitative asymptotic behaviors predicted here—damped oscillatory space-charge profiles with decay lengths significantly longer than the Debye length—to be present in a wide range of real-world solid electrolytes.

J. M. D. acknowledges support from the EPSRC (Grant No. 2119790). J. M. D. and B. J. M. acknowledge the support of the Faraday Institution through the Multi-Scale Modeling project (Grant No. FIRG003). S. W. C. and B. J. M. acknowledge the support of the Faraday Institution through the CATMAT project (Grant No. FIRG016). B. J. M. acknowledges support from the Royal Society (UF130329 and URF\R\191006). W. R. S., M. J. W., and A. B. W. acknowledge funding from the European Union's Horizon 2020 program, via the Energy Oriented Centre of Excellence (EoCoE-II), under grant agreement no. 676629. The authors thank Dr. Ian R. Thompson for useful discussions. We are grateful to the UK Materials and Molecular Modeling Hub for computational resources, which is partially funded by EPSRC (EP/P020194/1). This research made use of the Balena High Performance Computing (HPC) Service at the University of Bath.

Note added.—A dataset containing the full set of time-averaged simulation data that support the findings presented here and the analysis code used to generate Figs. 2 and 3 is available as Ref. [29] under the CC BY 4.0 and MIT licenses.

*Corresponding author.
swc57@bath.ac.uk
†Corresponding author.
b.j.morgan@bath.ac.uk

[1] J. Frenkel, *Kinetic Theory of Liquids* (Oxford University Press, New York, 1946).
[2] J. D. Eshelby, C. W. A. Newey, P. L. Pratt, and A. B. Lidiard, Charged dislocations and the strength of ionic crystals, Philos. Mag. **3**, 75 (1958).
[3] K. L. Kliewer and J. S. Koehler, Space charge in ionic crystals. I. General approach with application to NaCl, Phys. Rev. **140**, A1226 (1965).
[4] R. B. Poeppel and J. M. Blakely, Origin of equilibrium space charge potentials in ionic crystals, Surf. Sci. **15**, 507 (1969).
[5] Z. Cheng, M. Liu, S. Ganapathy, C. Li, Z. Li, X. Zhang, P. He, H. Zhou, and M. Wagemaker, Revealing the impact of space-charge layers on the Li-ion transport in all-solid-state batteries, Joule **4**, 1311 (2020).
[6] M. W. Swift, J. W. Swift, and Y. Qi, Modeling the electrical double layer at solid-state electrochemical interfaces, Nat. Comput. Sci. **1**, 212 (2021).
[7] J. Maier, Ionic conduction in space charge regions, Prog. Solid State Chem. **23**, 171 (1995).
[8] X. Xu, Y. Liu, J. Wang, D. Isheim, V. P. Dravid, C. Phatak, and S. M. Haile, Variability and origins of grain boundary electric potential detected by electron holography and atom-probe tomography, Nat. Mater. **19**, 887 (2020).
[9] K. K. Adepalli, J. Yang, J. Maier, H. L. Tuller, and B. Yildiz, Tunable oxygen diffusion and electronic conduction in $SrTiO_3$ by dislocation-induced space charge fields, Adv. Funct. Mater. **27**, 1700243 (2017).
[10] N. J. J. de Klerk and M. Wagemaker, Space-charge layers in all-solid-state batteries; important or negligible? ACS Appl. Energy Mater. **1**, 5609 (2018).
[11] E. E. Helgee, A. Lindman, and G. Wahnström, Origin of space charge in grain boundaries of proton-conducting $BaZrO_3$, Fuel Cells **13**, 19 (2013).
[12] A. Uthayakumar, A. Pandiyan, S. Mathiyalagan, A. K. Keshri, and S. B. K. Moorthy, The effect of space charge on blocking grain boundary resistance in an yttrium-doped barium zirconate electrolyte for solid oxide fuel cells, J. Phys. Chem. C **124**, 5591 (2020).
[13] The low space-charge potential limit is formally given by $\Phi_{sc} q \ll k_B T$, where Φ_{sc} is the "space-charge potential" at the interface, q is the charge of the mobile-defect species, k_B is the Boltzmann constant, and T is the temperature.
[14] X. Tong, D. S. Mebane, and R. A. De Souza, Analyzing the grain-boundary resistance of oxide-ion conducting electrolytes: Poisson–Cahn vs Poisson–Boltzmann theories, J. Am. Ceram. Soc. **103**, 5 (2020).
[15] D. S. Mebane, A variational approach to surface cation segregation in mixed conducting perovskites, Comput. Mater. Sci. **103**, 231 (2015).
[16] T. Patsahan, G. Bokun, D. di Caprio, M. Holovko, and V. Vikhrenko, The effect of short-range interaction and correlations on the charge and electric field distribution in a model solid electrolyte, Solid State Ionics **335**, 156 (2019).
[17] D. S. Mebane and R. A. De Souza, A generalised space-charge theory for extended defects in oxygen-ion conducting electrolytes: From dilute to concentrated solid solutions, Energy Environ. Sci. **8**, 2935 (2015).
[18] T. Bondevik, J. M. Polfus, and T. Norby, Disagreements between space charge models and grain boundary impedance data in yttrium-substituted barium zirconate, Solid State Ionics **353**, 115369 (2020).
[19] A. B. Walker and M. J. Gillan, Thermodynamics of the Coulomb lattice gas, J. Phys. C **16**, 3025 (1983).
[20] S. G. Brush, H. L. Sahlin, and E. Teller, Monte Carlo study of a one-component plasma. I, J. Chem. Phys. **45**, 2102 (1966).
[21] M. Baus and J.-P. Hansen, Statistical mechanics of simple Coulomb systems, Phys. Rep. **59**, 1 (1980).
[22] W. R. Saunders, J. Grant, E. H. Müller, and I. Thompson, Fast electrostatic solvers for kinetic Monte Carlo simulations, J. Comput. Phys. **410**, 109379 (2020).
[23] W. R. Saunders, J. Grant, and E. H. Müller, A domain specific language for performance portable molecular dynamics algorithms, Comput. Phys. Commun. **224**, 119 (2018).
[24] A. R. McCluskey and T. Snow, URAVU: Making Bayesian modelling easy(er), J. Open Source Software **5**, 2214 (2020).
[25] J. Skilling, Nested sampling, AIP Conf. Proc. **735**, 395 (2004).
[26] J. S. Speagle, DYNESTY: A dynamic nested sampling package for estimating Bayesian posteriors and evidences, Mon. Not. R. Astron. Soc. **493**, 3132 (2020).
[27] See Supplemental Material, which includes Ref. [28], at http://link.aps.org/supplemental/10.1103/PhysRevLett.127.135502 for a discussion of Fig. 2 when replotted on a semilogarithmic scale, a discussion of the choice of the nondimensional coupling parameter used in Fig. 3, and further details of the Bayesian analysis of the simulated space-charge profiles and subsequent parameter estimation.
[28] R. E. Kass and A. E. Raftery, Bayes factors, J. Am. Stat. Assoc. **90**, 773 (1995).
[29] J. M. Dean, S. W. Coles, W. R. Saunders, A. R. McCluskey, M. J. Wolf, A. B. Walker, and B. J. Morgan, Supporting dataset for "Overscreening and underscreening in solid-electrolyte grain boundary space-charge layers" (2021) https://doi.org/10.5281/zenodo.4647844.
[30] M. Z. Bazant, B. D. Storey, and A. A. Kornyshev, Double Layer in Ionic Liquids: Overscreening versus Crowding, Phys. Rev. Lett. **106**, 046102 (2011).
[31] J. Petersen and W. Dieterich, Effects of Coulomb interaction and disorder in a stochastic lattice gas, Philos. Mag. B **65**, 231 (1992).
[32] A. A. Lee, C. S. Perez-Martinez, A. M. Smith, and S. Perkin, Scaling Analysis of the Screening Length in Concentrated Electrolytes, Phys. Rev. Lett. **119**, 026002 (2017).
[33] A. A. Lee, C. S. Perez-Martinez, A. M. Smith, and S. Perkin, Underscreening in concentrated electrolytes, Faraday Discuss. **199**, 239 (2017).
[34] The possibility of solid electrolytes exhibiting oscillatory charge-profiles was previously highlighted by Gray-Weale [35], although this earlier analysis did not resolve the decay behavior of these oscillations.
[35] A. Gray-Weale, Screening and strain in superionic conductors, Faraday Discuss. **134**, 297 (2007).

[36] D. T. Limmer, Interfacial Ordering and Accompanying Divergent Capacitance at Ionic Liquid–Metal Interfaces, Phys. Rev. Lett. **115**, 256102 (2015).
[37] P. Attard, Asymptotic analysis of primitive model electrolytes and the electrical double layer, Phys. Rev. E **48**, 3604 (1993).
[38] A. M. Smith, A. A. Lee, and S. Perkin, The electrostatic screening length in concentrated electrolytes increases with concentration, J. Phys. Chem. Lett. **7**, 2157 (2016).
[39] R. M. Adar, S. A. Safran, H. Diamant, and D. Andelman, Screening length for finite-size ions in concentrated electrolytes, Phys. Rev. E **100**, 042615 (2019).
[40] S. W. Coles, C. Park, R. Nikam, M. Kanduč, J. Dzubiella, and B. Rotenberg, Correlation length in concentrated electrolytes: Insights from all-atom molecular dynamics simulations, J. Phys. Chem. B **124**, 1778 (2020).
[41] D. D. Carley, Computations of radial distribution functions for a classical electron gas, Phys. Rev. **131**, 1406 (1963).
[42] B. Rotenberg, O. Bernard, and J.-P. Hansen, Underscreening in ionic liquids: A first principles analysis, J. Phys.: Condens. Matter **30**, 054005 (2018).
[43] L. Ornstein and F. Zernike, Accidental deviations of density and opalescence at the critical point of a single substance, Proc. R. Net. Acad. Art. Sci. **17**, 793 (1914), https://www.dwc.knaw.nl/DL/publications/PU00012727.pdf.
[44] F. Coupette, A. A. Lee, and A. Härtel, Screening Lengths in Ionic Fluids, Phys. Rev. Lett. **121**, 075501 (2018).
[45] J. G. Kirkwood, Statistical mechanics of liquid solutions, Chem. Rev. **19**, 275 (1936).
[46] J. Ennis, R. Kjellander, and D. J. Mitchell, Dressed ion theory for bulk symmetric electrolytes in the restricted primitive model, J. Chem. Phys. **102**, 975 (1995).
[47] R. Kjellander, The intimate relationship between the dielectric response and the decay of intermolecular correlations and surface forces in electrolytes, Soft Matter **15**, 5866 (2019).
[48] R. Kjellander, Focus article: Oscillatory and long-range monotonic exponential decays of electrostatic interactions in ionic liquids and other electrolytes: The significance of dielectric permittivity and renormalized charges, J. Chem. Phys. **148**, 193701 (2018).
[49] P. Cats, R. Evans, A. Härtel, and R. van Roij, Primitive model electrolytes in the near and far field: Decay lengths from DFT and simulations, J. Chem. Phys. **154**, 124504 (2021).
[50] M. V. Fedorov and A. A. Kornyshev, Ionic liquids at electrified interfaces, Chem. Rev. **114**, 2978 (2014).
[51] A. A. Kornyshev, Double-layer in ionic liquids: Paradigm change? J. Phys. Chem. B **111**, 5545 (2007).
[52] S. Perkin, T. Albrecht, and J. Klein, Layering and shear properties of an ionic liquid, 1-ethyl-3-methylimidazolium ethylsulfate, confined to nano-films between mica surfaces, Phys. Chem. Chem. Phys. **12**, 1243 (2010).
[53] M. A. Gebbie, M. Valtiner, X. Banquy, E. T. Fox, W. A. Henderson, and J. N. Israelachvili, Ionic liquids behave as dilute electrolyte solutions, Proc. Natl. Acad. Sci. U.S.A. **110**, 9674 (2013).
[54] M. A. Gebbie, H. A. Dobbs, M. Valtiner, and J. N. Israelachvili, Long-range electrostatic screening in ionic liquids, Proc. Natl. Acad. Sci. U.S.A. **112**, 7432 (2015).
[55] R. Evans and T. Sluckin, A density functional theory for inhomogeneous charged fluids, Mol. Phys. **40**, 413 (1980).
[56] R. L. de Carvalho and R. Evans, The decay of correlations in ionic fluids, Mol. Phys. **83**, 619 (1994).
[57] R. Evans, J. Henderson, D. Hoyle, A. Parry, and Z. Sabeur, Asymptotic decay of liquid structure: Oscillatory liquid-vapour density profiles and the Fisher–Widom line, Mol. Phys. **80**, 755 (1993).
[58] A. A. Lee, D. Vella, S. Perkin, and A. Goriely, Are room-temperature ionic liquids dilute electrolytes? J. Phys. Chem. Lett. **6**, 159 (2015).
[59] P. Jones, F. Coupette, A. Härtel, and A. A. Lee, Bayesian unsupervised learning reveals hidden structure in concentrated electrolytes, J. Chem. Phys. **154**, 134902 (2021).
[60] R. A. D. Souza, Z. A. Munir, S. Kim, and M. Martin, Defect chemistry of grain boundaries in proton-conducting solid oxides, Solid State Ionics **196**, 1 (2011).
[61] J. M. Polfus, K. Toyoura, F. Oba, I. Tanaka, and R. Haugsrud, Defect chemistry of a $BaZrO_3$ $\Sigma 3$ (111) grain boundary by first principles calculations and space-charge theory, Phys. Chem. Chem. Phys. **14**, 12339 (2012).
[62] J.-H. Yang, B.-K. Kim, and Y.-C. Kim, Calculation of proton conductivity at the $\Sigma 3(111)/[1\bar{1}0]$ tilt grain boundary of barium zirconate using density functional theory, Solid State Ionics **279**, 60 (2015).
[63] M. Mottet, A. Marcolongo, T. Laino, and I. Tavernelli, Doping in garnet-type electrolytes: Kinetic and thermodynamic effects from molecular dynamics simulations, Phys. Rev. Mater. **3**, 035403 (2019).
[64] S. P. Culver, A. G. Squires, N. Minafra, C. W. F. Armstrong, T. Krauskopf, F. Böcher, C. Li, B. J. Morgan, and W. G. Zeier, Evidence for a solid-electrolyte inductive effect in the superionic conductor $Li_{10}Ge_{1-x}Sn_xP_2S_{12}$, J. Am. Chem. Soc. **142**, 21210 (2020).
[65] A. Lindman, E. E. Helgee, B. J. Nyman, and G. Wahnström, Oxygen vacancy segregation in grain boundaries of $BaZrO_3$ using interatomic potentials, Solid State Ionics **230**, 27 (2013).
[66] T. Bondevik, T. S. Bjørheim, and T. Norby, Assessing common approximations in space charge modelling to estimate the proton resistance across grain boundaries in Y-doped $BaZrO_3$, Phys. Chem. Chem. Phys. **22**, 11891 (2020).
[67] S. Grieshammer, B. O. H. Grope, J. Koettgen, and M. Martin, A combined DFT + U and Monte Carlo study on rare earth doped ceria, Phys. Chem. Chem. Phys. **16**, 9974 (2014).
[68] S. Stegmaier, J. Voss, K. Reuter, and A. C. Luntz, Li^+ defects in a solid-state li ion battery: Theoretical insights with a Li_3OCl electrolyte, Chem. Mater. **29**, 4330 (2017).